Laser Texturing of Soda-Lime Glass Surfaces with Extreme Wettability Contrast

Marcos Soldera[*1], Fabian Ränke[1], and Andrés Fabián Lasagni[1,2]

[1]*Institute of Manufacturing, Technische Universität Dresden, 01062 Dresden, Germany*
[2]*Fraunhofer Institute for Material and Beam Technology IWS, 01277 Dresden, Germany*
[*]*Corresponding author's e-mail: marcos.soldera@tu-dresden.de*

The ability to create extreme wettability contrast on glass surfaces has significant implications for applications such as self-cleaning systems, fluid manipulation, anti-fogging, and open-surface microfluidics. However, achieving this contrast in a controllable manner remains challenging. In this study, soda-lime glass surfaces are engineered with extreme wettability properties following a two-step approach. First, laser ablation using either Direct Laser Writing (DLW) or Direct Laser Interference Patterning (DLIP) based on a ns-pulsed UV (266 nm) source was used to microtexture glass with single-scale or hierarchical patterns. Due to the increased roughness, the laser-treated surfaces become superhydrophilic with water contact angles below 10°. To induce hydrophobicity, the laser-textured surfaces are subsequently sprayed with a hydrophobizing agent based on a chemically active perfluoropolyether compound. This process converts all hydrophilic surfaces into highly hydrophobic ones, exhibiting water contact angles exceeding 140° for the hierarchical surfaces. Surface free energy (SFE) measurements revealed highly inert hydrophobic surfaces with SFE values below 1 mN/m, while values exceeding 80 mN/m were obtained for the superhydrophilic glass. Finally, the potential of glass surfaces with extreme wetting contrast is demonstrated by fabricating superhydrophilic channels surrounded by hydrophobic areas that are able to spontaneously transport water.

DOI: 10.2961/jlmn.2025.02.2008
Keywords: Direct Laser Interference Patterning, Direct Laser Writing, glass microstructuring, UV-laser, wettability contrast, surface free energy

1. Introduction

Surface wettability is a critical parameter in the performance and functionality of many glass-based devices and systems [1,2]. Soda-lime glass, widely used in optical components, architecture, and microfluidic substrates, is inherently hydrophilic with water contact angles (WCA) in the range of 20 to 50° [3,4], due to its polar surface chemistry and smooth morphology. However, in many advanced applications, controlling or spatially tuning the wettability of glass surfaces is essential. For example, precise wettability control enables fluid manipulation in open-surface microfluidics [5,6], anti-fogging [7], fog-collection [8] and self-cleaning [9] functions and selective adsorption or repulsion of biomolecules in diagnostic platforms [10]. Particularly, surfaces that exhibit extreme wettability contrast, i.e., the coexistence of superhydrophilic (WCA <10°) and superhydrophobic (WCA >150°) regions, offer enhanced functionalities by enabling new fluid-control schemes (droplet pumping, directional wetting, oil–water separation, etc.) across chemical, optical, and biological devices [11–13]. Engineering such wettability contrast directly on glass, while preserving optical quality and mechanical integrity, remains a technical challenge requiring precise surface modification techniques.

Previous studies have been dedicated to explore the fabrication of glass surfaces with either strong hydrophilic or hydrophobic properties. Yu et al. employed a CF_4 plasma etching approach for obtaining nanopatterns that promoted superhydrophilicity. Upon depositing a hydrophobizing coating by PECVD, the patterned surface turned superhydrophobic [14]. In another work, glass surfaces were treated by flame impingement to repolymerize bridging oxygens acting as adsorption sites for water and thus promoting superhydrophilicity [15]. Similarly, Zhang et al. annealed soda-lime glasses at 900 K to turn the surface superhydrophilic by promoting the formation of oxide species on the surface [16]. In a different study, glass slides were patterned by atmospheric-pressure plasma jet using different type of precursor gases (plasma-polymerized hexamethyldisiloxane and acrylic acids) to obtain the different wettability states [17].

Although these methods succeeded in achieving extreme wettability states, they are not flexible enough for modulating the local wetting properties, unless masks are used.

Laser-based technologies can overcome this limitation, as they are versatile methods for fabricating intricate surface patterns and they can be easily adapted between or within processing batches. Furthermore, they do not require masks and typically need less pre- or post-processing steps than other methods for a targeted application. Laser ablation has been demonstrated to be an effective method for increasing surface roughness on glass substrates [18–21]. This can induce a saturated Wenzel state, whereby the

water infiltrates all the protrusions and asperities of the surface and increase strongly the glass wettability [7,22]. Likewise, some reports have shown the increase of water contact angle towards the hydrophobic region (WCA > 90°) by inducing a Cassie-Baxter-like state through the patterning of features with a typical pitch size in the order of 100 µm [23–26]. However, to induce a strong hydrophobic, or superhydrophobic, wetting state the common procedure is to combine an adequate surface topography with specific chemical modifications. Following this strategy, several studies reported the fabrication of (super)-hydrophobic surfaces by laser ablation followed by the deposition of a functional layer, such as silicone oil, Teflon-like polymer or silane-based solution [3,11,27]. Despite the high hydrophobicity achieved, these methods still require multiple steps or the use of fs-pulsed laser sources. It is also worth to mention the work by Dinh et al., in which they achieved superhydrophobic soda-lime glass by patterning grid-like arrays using a ns-laser (UV) followed by an annealing step [28]. However, this process has the drawback that the heat treatment takes 48 h, representing a limitation for high-throughput applications. A significant enhancement of the productivity was achieved in the work by Wang et al., in which the laser-treated glass was hydrophobized by a silicon oil-assisted heat treatment combined with several ultrasonic bath steps, reducing the post-treatment step to 20 min [3].

In this work, we present a two-step approach to fabricate soda-lime glass with locally modulated hydrophobic and hydrophilic regions. The first step is based on laser micromachining using a UV (266 nm) source emitting ns-pulses by either Direct Laser Writing (DLW), i.e., single-beam ablation, or Direct Laser Interference Patterning (DLIP). As DLIP allows the fabrication of periodic textures with spatial periods on the order of a few µm, periodic textures across different scales are produced. Furthermore, by adjusting the DLIP parameters, hierarchical textures are also fabricated. For increasing the water-repellency on the textured samples, a hydrophobizing coating is applied by mask-free spray deposition. The glass surfaces are then characterized by scanning electron and confocal microscopy, and by measuring the static water contact angle and surface free energy.

2. Materials and methods

2.1 Materials

Soda-lime glass plates (100 mm × 100 mm × 5 mm) fabricated by the float-glass method (Aachener Quarzglas-Technologie Heinrich GmbH & Co. KG, Germany) were used in this study. This type of glass has a high resistance to almost all acids, salts, and their solutions and has remarkable thermal, optical, and mechanical properties, which make it a commonly used all-purpose and low-cost glass.

2.2 Laser surface texturing setup

An in-house developed Direct Laser Interference Patterning (DLIP) (TU Dresden and Laservorm GmbH, Germany) setup was used for the microtexturing experiments. The UV (266 nm) laser source (Compact Laser Solutions GmbH, Germany) emitted ns-pulses at a fixed repetition rate of 38 kHz and maximum power of 3 W. The setup is coupled to a galvoscanner (intelliSCAN III 14, Scanlab GmbH, Germany) and an f-theta lens (JENar 03-71FT-103-266, Jenoptik AG), which yield a scan field of 50 × 50 mm^2 and a maximum mark speed of 3.1 m/s.

The DLIP method was implemented by splitting the primary beam into two sub-beams by a diffractive optical element (DOE). The sub-beams were directed to a prism to parallelize them and then guided to the scanner aperture. Finally, the sub-beams are overlapped on the sample surface by the f-theta lens. A sketch of the setup is shown in Figure 1. The overlapping angle and thus the periodicity of the interference pattern can be controlled by adjusting the distance between the DOE and prism. In this study, a fixed spatial period of 3.3 µm was used. The parameters for the DLIP process were the scanner speed, which was varied between 0.6 m/s and 1.8 m/s and the number of passes, which was swept from 1 to 5. The average fluence and spot diameter were kept fixed at 3.1 J/cm^2 and 40 µm, respectively. Likewise, the hatch distance was set to 26 µm for all DLIP experiments.

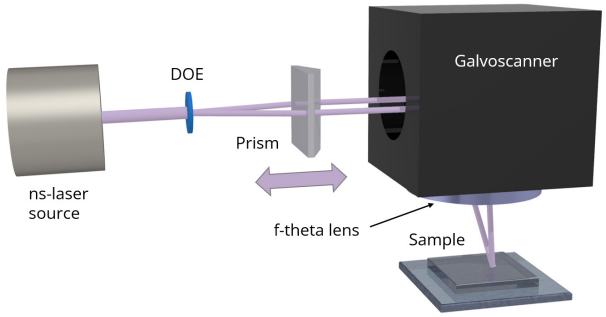

Fig. 1 Sketch of DLIP setup based on a ns-laser source and a galvoscanner. See text for details.

The same scanner system was used for the Direct Laser Writing (DLW) method. In this case, dot-like structures were patterned by moving the beam at a constant speed of 1.14 m/s at 38 kHz, resulting in a distance between craters of 30 µm. The number of pulses per spot was varied from 1 to 12 by controlling the number of overscans and the average fluence was kept constant at 1.5 J/cm^2.

2.3 Surface chemistry modification

To induce hydrophobicity, selected laser-textured glass surfaces were subsequently sprayed with a hydrophobizing agent based on a chemically active perfluoropolyether compound dissolved in a fluorinated solvent (Mecasurf, Surfactis Technologies, France).

2.4 Characterization methods

Scanning electron microscopy (Quattro ESEM, Thermo Fischer Scientific, Germany) images were taken on Au-coated glass samples at an acceleration voltage of 5 kV. Furthermore, the topography was measured by confocal microscopy (Sensofar S-Neox, Spain) using a 150x objective, with a lateral and vertical resolution of 140 nm and 1 nm, respectively.

The wettability of the fabricated surfaces was characterized by measuring the static contact angle of deionized (DI) water droplets with a volume of 2 µl using a drop shape analyzer (Krüss DSA 100 S, Germany). Additionally, the surface free energy of the samples was estimated using

the Owens-Wendt-Rabel-Kaelbel (OWRK) method by measuring the contact angles of DI water (polar liquid) and diiodomethane (non-polar) [29]. Each measurement was repeated at least 5 times for statistical significance. The surface tension for the two testing liquids used in this study, as well as their dispersive γ^D and polar γ^P components are given in Table 1.

Table 1 Surface tension of used test liquids at 298 K.

Test liquids	Surface tension [mN/m]	Polar γ^P [mN/m]	Dispersive γ^D [mN/m]
Deionized water	72.8	51.0	21.8
Diiodomethane	50.8	0.0	50.8

3. Results and discussion

3.1 Fabrication of microstructures on glass

In this study, UV (266 nm) ns-pulses were used to structure soda-lime glass surfaces as this material has a strong absorption at this wavelength. Using the DLIP configuration, two structuring regimes were identified according to the used scanner speed, or equivalently pulse-to-pulse distance d_{p2p}. Selected SEM images of surfaces treated with a single pass at speeds ranging from 0.6 to 1.1 m/s, corresponding to the low-speed regime, are shown in Figure 2 (the labels indicate the scanner speed, *S*). The images reveal a line-like topography with straight grooves separated by the texture spatial period of 3.3 µm (in agreement with the optical configuration used). In all cases, nanoparticles distributed over the surfaces can be observed as a by-product of the laser ablation. The glass surface shown in Figure 2a was structured with the lowest speed in this study (0.6 m/s) which corresponds to a pulse-to-pulse distance d_{p2p} of 16 µm. In this case, cracks predominantly propagating across the grooves, namely across the structuring direction, become evident. As the scanner speed increases to 0.9 m/s (d_{p2p} = 24 µm) no signs of cracks could be detected (Figure 2b), and the texture shows good overall uniformity. This observation is also valid for the sample textured at a speed of 1.1 m/s (d_{p2p} = 29 µm), shown in Figure 2c, although the textures turned shallower. In this low-speed regime, it was observed that multiple overscans resulted in excessive cumulated fluence, leading to overmelting, poorly-defined periodic textures and extensive coverage of cracks (not shown here) and therefore only samples with one pass were considered in this regime for wettability analysis.

As the scanner speed is increased beyond 1.2 m/s, the pulse-to-pulse distance approach the spot size of 40 µm and thus the pulse-to-pulse overlaps are less than 25%. This strategy gives rise to the second structuring, or high-speed, regime, where the textures are characterized by a hierarchical topography consisting of DLIP grooves (similar as the surfaces shown in Figure 2) combined with craters as observed in the selected SEM images of Figure 3 (the labels correspond to the scanner speed *S* and number of passes *N*). As the scanning speed increases, the craters become more widely spaced along the structuring direction (i.e., the groove direction). This can be observed upon comparing the textures structured at 1.2 m/s (Figures 3a-c) with those patterned at 1.6 m/s (Figure 3d-f). Apart from the mentioned separation between the craters, no other effects were identified upon changing the speed. In turn, the number of passes has a strong influence on the morphology as more cumulated fluence tends to yield deeper structures and eventually significant heat-related effects such as the initiation of cracks. Interestingly, as the number of passes increase the cracks tend to propagate along random directions and not only perpendicular to the grooves as observed in the surfaces of Figure 2.

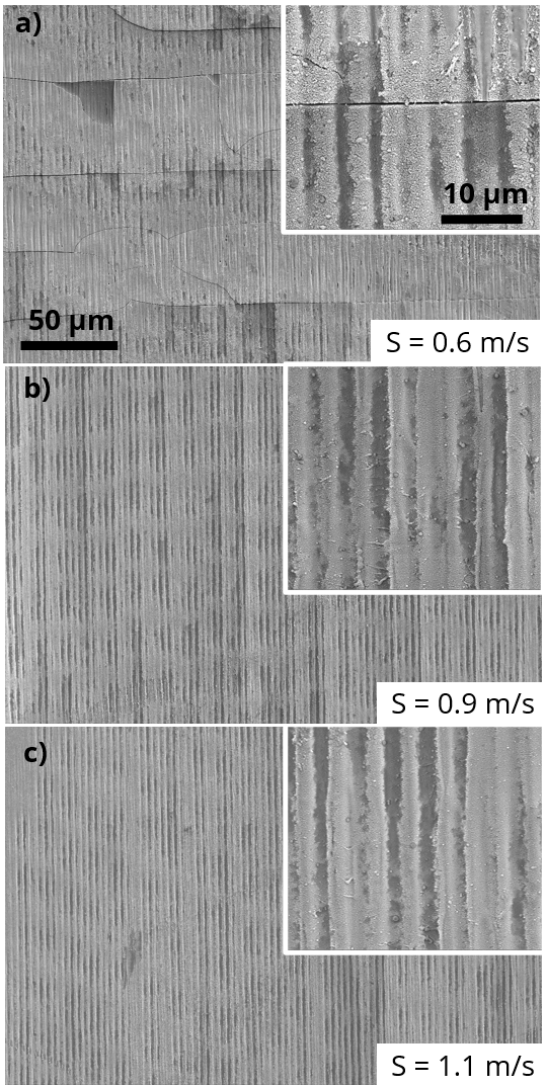

Fig. 2 Selected SEM images of soda-lime glass structured using DLIP with a single pass at a scanner speed *S* of a) 0.6 m/s, b) 0.9 m/s, and c) 1.1 m/s. All samples present a single-scale texture featuring a line-like pattern.

The same approach was used in case of DLW. Figure 4 shows selected SEM images of surfaces treated with different number of passes *N* (see labels). Figure 4a displays the surface treated with a single pass, showing regularly spaced craters surrounded by a rim, probably corresponding to the solidified melt front. In this sample, the craters have a smooth topography and no redeposited debris or cracks are visible. These characteristics are still present as the number of passes increase to four (not shown here). In turn, as the number of passes further increases, for example N = 8 as shown in Figure 4b, the craters not only become deeper but also other features appear, such as solidified splashes, redeposited nanoparticles and eventually

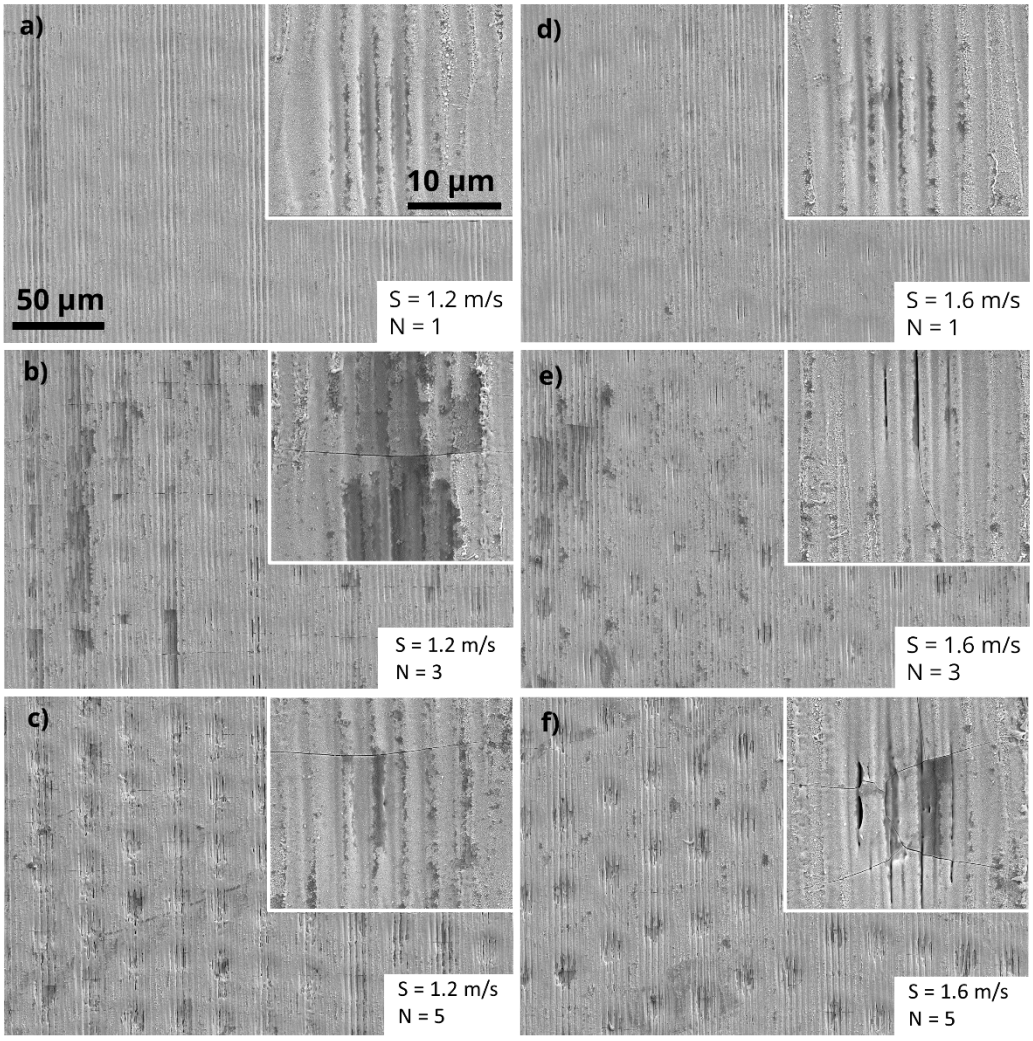

Fig. 3 Selected SEM images of soda-lime glass structured using DLIP at different scanner speed *S* and number of passes *N* (see labels). In all images, a hierarchical texture consisting of a line-like pattern combined with a regular array of craters can be observed.

cracks. At high number of passes, for instance $N = 14$ (Figure 4c), the craters are surrounded by a significant amount of resolidified material and cracks become predominant.

Confocal microscopy analysis allowed the estimation of the structure heights of the produced grooves and craters. Figure 5a shows the calculated height as function of the used scanner speed of the DLIP-treated glass surfaces and with the number of passes as parameter. The vertical dashed line separates the identified regimes which in turn distinguish the speeds at which single-scale or hierarchical textures characterize the surface topography. In general, the DLIP structure height increases with decreasing speed, or equivalently decreasing pulse-to-pulse distance. As expected, the height also increases with the number of passes [30].

As shown in Figure 5b, the structure height of the craters increases practically linearly with the number of passes for the DLW-treated surfaces. To estimate the depth of the craters in the hierarchical textures fabricated by DLIP in the high-speed regime, a gaussian filter was applied to extract the waviness. This value is plotted in Figure 5b as the structure height as function of the scanner speed and number of passes. The depths of the craters produced by DLIP increase similarly to those fabricated by DLW, although for a few conditions, they are significantly deeper than on the equivalent DLW samples.

3.2 Wettability characterization

To study the wetting characteristics of the laser-treated glass surfaces, static water contact angle (WCA) was measured on the samples after fabrication. Figure 6 shows the average value of WCA and its standard deviation (error bars) of the DLIP treated surfaces, as function of scanner speed and number of passes (green bars). As mentioned in the previous section, in the low-speed regime (i.e., $S < 1.2$ m/s) single-scale textures were identified for a single pass. Multiple passes in this regime led to damaged textures and therefore their wetting properties were not evaluated. In all cases, the surfaces turned even more hydrophilic than the untreated surface (green dashed line), and in many cases the surfaces became superhydrophilic (WCA < 10°) and completely wetted the structured area (1 cm^2). In agreement with similar experimental works found in the literature, the increase of hydrophilicity can be directly correlated to the increased surface roughness, which induced a saturated Wenzel state [3]. Particularly, for the hierarchical structures fabricated with 4 and 5

passes, all samples were superhydrophilic regardless of the scanner speed.

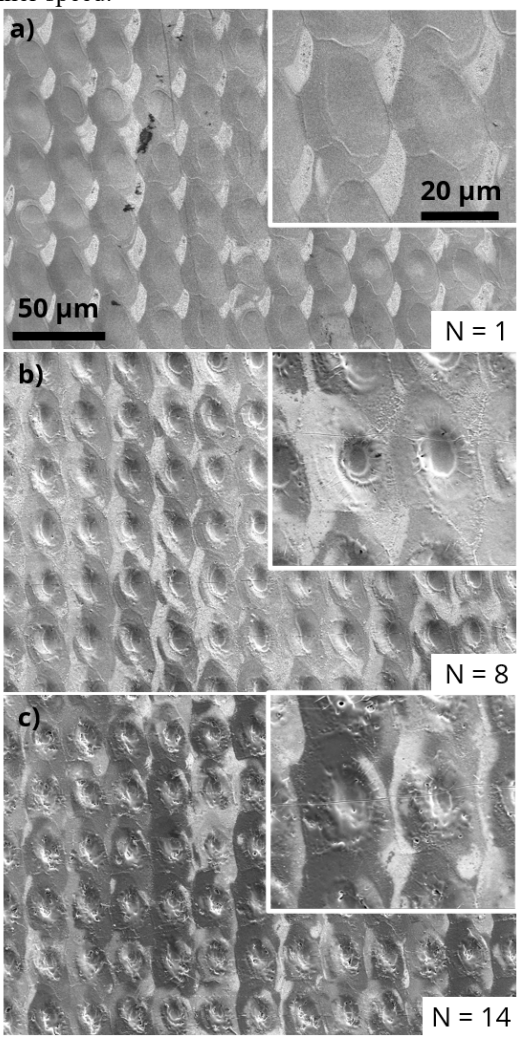

Fig. 4 Selected SEM images of DLW-treated glass surfaces with different number of passes *N* (see labels). The surfaces are characterized by a square array of craters, that become deeper as the number of passes increases.

To make the laser-treated surfaces hydrophobic, they were sprayed with a perfluoropolyether compound dissolved in a fluorinated solvent, with the commercial name Mecasurf. As shown in Figure 6, the treated samples exhibited a substantial increase in water contact angle (WCA), becoming more hydrophobic than the untreated glass (WCA = 40°, indicated by the green dashed line). Except for the surfaces treated at a speed of 1.8 m/s with 1 and 2 passes, all other samples became more hydrophobic than the bare glass treated with Mecasurf (WCA = 89°, dashed orange line). Interestingly, the hierarchical textures produced with 4 and 5 passes and speeds of 1.2 and 1.4 m/s showed WCA above 140° and approaching 150°, which is the threshold value for superhydrophobicity. These hierarchical textures have a crater depth according to Figure 5b between 1.0 µm and 1.6 µm, and a DLIP groove height between 0.55 µm and 0.81 µm, which are the largest for the hierarchical structures.

The measurements on the single-scale DLIP textures showed very large standard deviations, both with and without Mecasurf, probably due to the low uniformity, especially at the lowest speeds, where heat accumulation effects, such as cracks, become predominant. Although the measurements for each treated surface were done at different observation angles for accounting for possible asymmetries of the droplets' shape due to the one-dimensional DLIP texture, no significant anisotropic effects were detected.

Also, static WCA were measured on the DLW-treated glass surfaces, exhibiting a superwetting behavior for all number of passes (Figure 7). In the case of the Mecasurf sprayed surfaces, although the samples turned hydrophobic, the average WCA were not as high as the hierarchical structures, namely, they remained below 135°. The highest WCA was obtained for 2 and 4 passes, which corresponds to structure heights of 0.44 µm and 1.07 µm, respectively. Deeper craters favored lower contact angles (between 85° and 115°), probably due to the appearance of randomly distributed debris and re-solidified material, that increased the wetting of the surface.

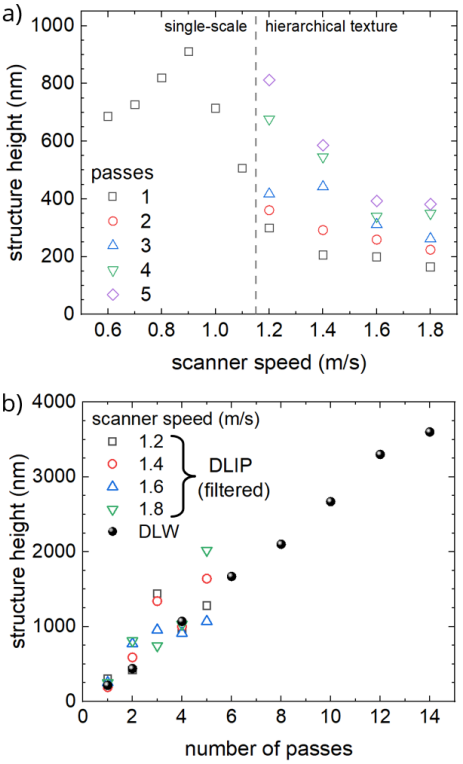

Fig. 5 a) Heights of the DLIP structures, i.e., grooves, calculated by confocal microscopy. b) Heights of the structures, i.e., craters, produced by DLW (solid spheres) and by DLIP (open symbols) after applying a gaussian filter (see text for details).

The surface free energy was measured on selected DLIP- and DLW-treated samples and shown in Figure 8a and b, respectively. The total (SFE) together with the polar and dispersive components were calculated. The DLIP samples correspond to those fabricated at a fixed speed of 1.2 m/s and thus belong to the high-speed, or hierarchical, regime. This speed was selected for these measurements as the samples exhibited superhydrophilic properties without the coating, and a wide range of WCA from 95° to 145°, depending on the number of passes, with the hydrophobizing coating (see Figure 6).

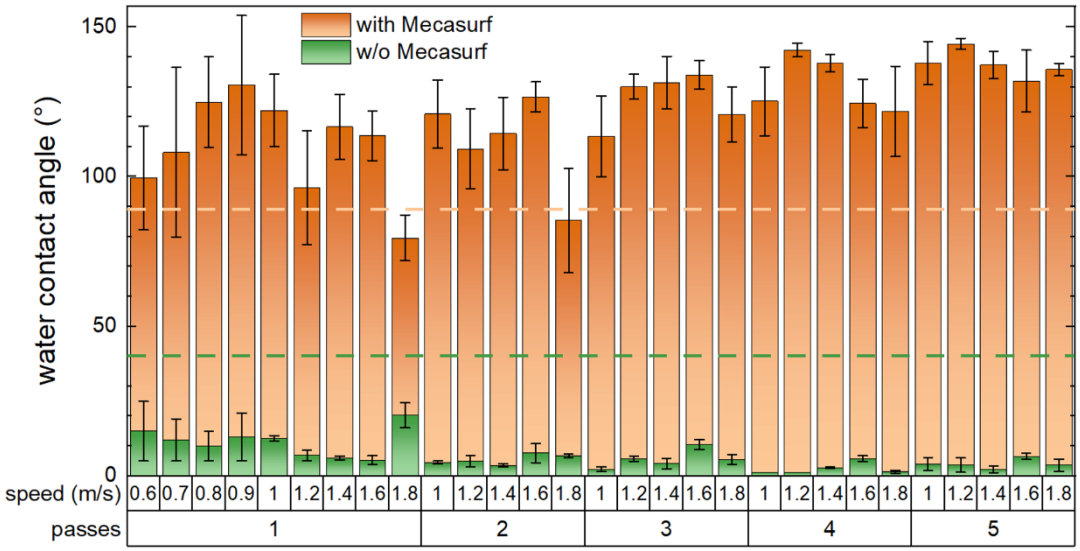

Fig. 6 Water contact angles measured on the DLIP-treated glass surfaces (green bars) and on the DLIP-textured and coated samples (orange bars) as function of the scanner speed and number of passes. As reference, the contact angle on untreated flat soda-lime glass (dashed green line) and on the coated flat surface (orange dashed line) are shown.

The SFE of the reference soda-lime, as well as its polar and dispersive components, are in agreement with the values reported in the literature, confirming the consistency of the employed method [24,31]. Upon spraying the coating, both components of the surface energy of the flat glass (Ref.) drop strongly, corresponding to an increase in the contact angle of water and di-iodomethane droplets. In the case of the DLIP-treated surfaces at a scanner speed of 1.2 m/s, the uncoated surfaces became superhydrophilic and kept this wetting state independent of the number of passes (see Figure 6), which can be explained by the significant increase in the SFE to approximately 80 mN/m on all textured samples. On the contrary, the coated surfaces become more hydrophobic as the number of passes increases. This observation aligns with the steady drop in the SFE as the number of passes increases, which is mainly driven by the reduction of its polar component. In all cases, spraying the coating on the samples induced a strong repellency of water and di-iodomethane droplets, which hints that the surfaces have omniphobic properties. Further tests with other liquids, such as oils, are required to confirm this hypothesis.

In the case of the DLW-treated samples without coatings, the SFE also reached a value of approximately 80 mN/m for all number of passes. In the case of $N = 12$, the dispersive component was larger than all other laser-treated surfaces, driven by the higher contact angles of di-iodomethane. When the coating is applied, the SFE drops strongly to values below 10 mN/m, except for the sample irradiated with 12 passes. This surface exhibited a higher polar component than all other laser-treated and coated surfaces, which can be correlated with the relatively low WCA of 85° (Figure 7).

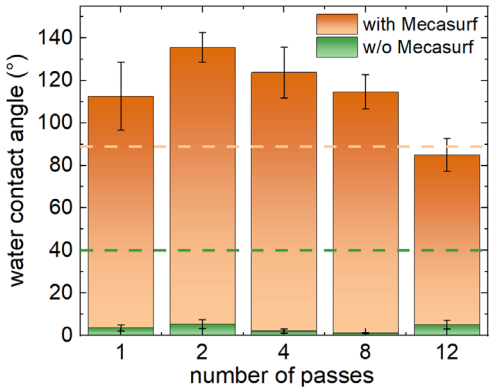

Fig. 7 Water contact angles measured on the DLW-structured glass surfaces (green bars) and on the DLW-textured and coated samples (orange bars) as function of number of passes. As reference, the contact angle on untreated flat soda-lime glass (dashed green line) and on the coated flat surface (orange dashed line) are shown.

3.3 Fabrication of surfaces with extreme wettability contrast

As discussed in the previous section, the wettability of soda-lime glass surfaces can be tuned, even reaching extreme WCA values, by combining laser texturing and coating with a hydrophobizing agent. Particularly, structuring hierarchical textures with the DLIP method at a scanning speed of 1.2 m/s and 4 passes was shown to provide a super-wetting state (WCA ~ 0°). After spraying the coating, this surface reached a WCA of 144°, the highest among the produced samples in this work. The versatility of the used laser texturing methods can be therefore exploited for designing patterns with local and tunable wetting properties. For instance, it is possible to fabricate superhydrophilic channels surrounded by hydrophobic areas, so that the water can only wet and propagate through the patterned channels. This water guidance application is demonstrated next by patterning the spiral-like channel shown in Figure 9, according to the following sequence:

- The area corresponding to the gray color shown in Figure 9 was patterned by DLIP ($S = 1.2$ m/s and $N = 4$), by scanning the sub-beams along the y-direction and by modulating the laser firing by the galvoscanner interface. Once a single track is finished, the sub-beams are displaced along the x-direction a distance (hatch) of 26 µm. In this way, the microgrooves arising from the DLIP treatment are oriented in the y-direction over all the structured area.
- Then, the glass substrate was uniformly sprayed with the Mecasurf® compound to increase the hydrophobicity.
- Finally, the spiral (black area in Figure 9) was patterned with the same laser parameters as in the first step ($S = 1.2$ m/s and $N = 4$), to remove the coating and simultaneously structure the surface to obtain the superhydrophilic texture. Analogously to the DLIP processing of the gray area of Figure 9, the microgrooves are oriented parallel to the y-direction and the laser firing was controlled by the galvoscanner software.

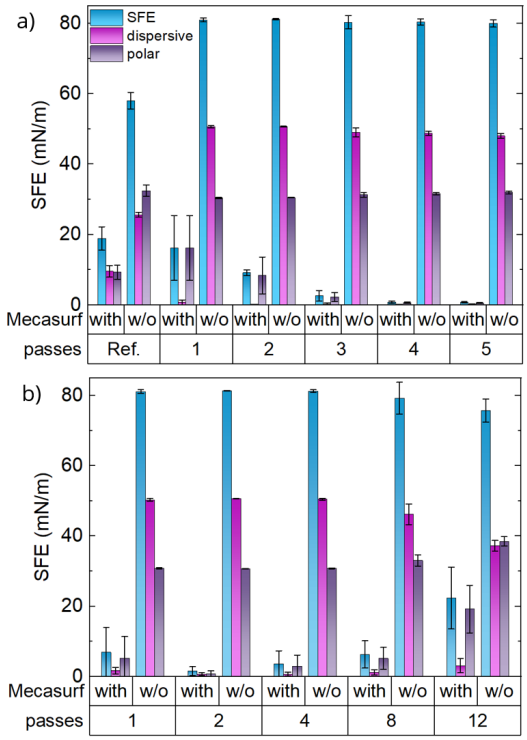

Fig. 8 Calculated surface free energy (SFE) along with its dispersive and polar components for the a) DLIP-treated (at a speed of 1.2 m/s) and b) DLW-textured glass surfaces with and without (w/o) the coating. In a) the reference (Ref.) values for the flat glass with and without the coating are also shown.

The used DLIP parameters yield the line-like pattern with the hierarchical morphology shown in the SEM image of Figure 10. The structure size corresponding to the grooves and craters heights can be found in Figure 5a and b, respectively.

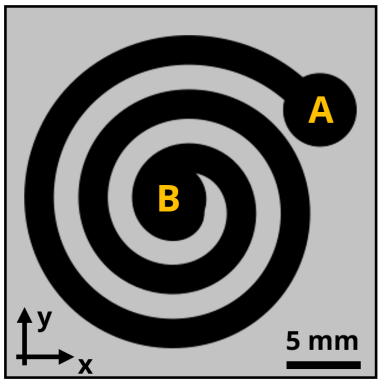

Fig. 9 Drawing of the patterned spiral-like channel with superhydrophilic property (black area) surrounded by hydrophobic regions (gray area).

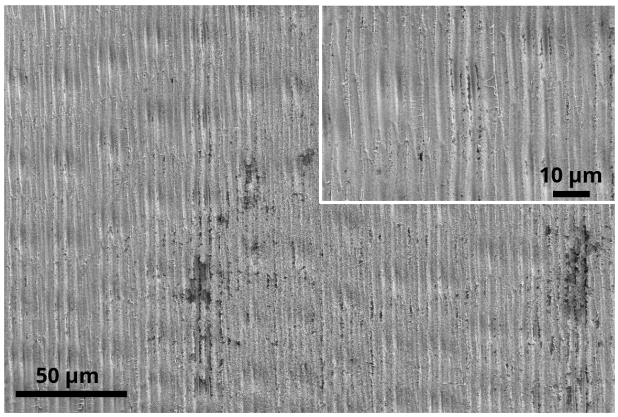

Fig. 10 SEM images of the DLIP-patterned surface of the soda-lime glass demonstrator using a scanner speed of 1.2 m/s and 4 passes.

To test this demonstrator, the glass plate was placed on the drop shape analyzer and water was continuously dispensed from a syringe at a rate of 1 µl/s on the reservoir A (also indicated in Figure 9). As the snapshots of Figures 11a-c show, the water is forced to propagate through the superhydrophilic channels as it cannot wet the hydrophobic area. After approximately 60 s, the water arrives at reservoir B in the center of the spiral. Considering that the channel length is approximately 103 mm, the average speed of the water motion can be estimated at 1.7 mm/s.

At the used laser parameters, the DLIP steps took 81 s each, yielding a structuring throughput of 4.3 cm^2/min per DLIP step. Between the structuring steps, the sample was taken out from the setup, sprayed with the hydrophobizing coating and left 30 s for drying in ambient conditions before placing the sample in the setup for the second DLIP step. Consequently, the total process time took approximately 230 s, providing a total throughput of 1.5 cm^2/min for this particular application. Furthermore, optimization of the structuring strategy, spraying procedure and structured geometry is required to increase this value closer to industrial standards.

This demonstrator serves not only to highlight the potential of glass surfaces with extreme wettability contrast but also can trigger further research on the influence of the geometrical parameters of the channels on the liquid flow, which can be attractive for open-surface microfluidics, lab-on-a-chip devices and fog collectors, as well as other

applications in which controlled liquid manipulation is required.

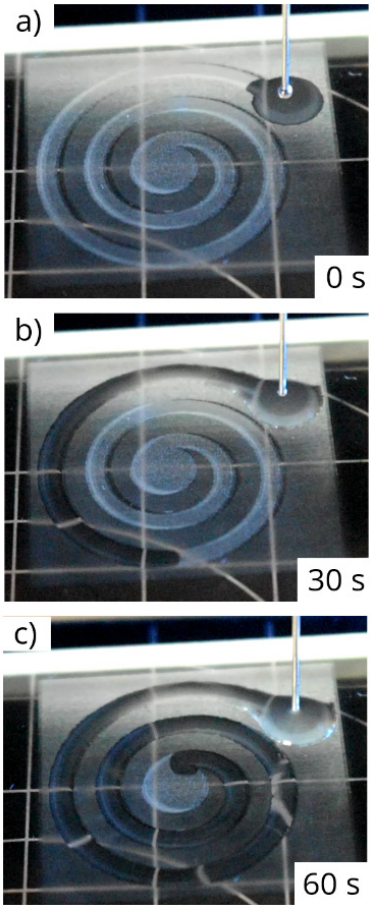

Fig. 11 Snapshots of the glass structured with extreme wettability contrast demonstrating the controlled liquid transport through the channel.

4. Conclusions

In this contribution, the patterning of soda-lime glass surfaces using a UV ns-laser source coupled to either DLIP or DLW configurations was investigated. By varying the laser parameters, namely pulse-to-pulse distance or number of overscans, different geometrical microtextures were achieved. The wettability of the surfaces was investigated by measuring the static water contact angle and the free surface energy of the samples as-produced as well as coated with a hydrophobizing agent. The results showed that the wettability can be significantly modified with these treatments. For instance, all laser-treated samples turned more hydrophilic than the reference, even reaching the superhydrophilic state, whereby the water completely wets the whole structured area. On the contrary, the application of the coating turned all samples hydrophobic and particularly for the hierarchical samples the water contact angles exceeded 140°. The extremely different values of the water contact angle could be explained by the strong modification of the free surface energy of the samples. The laser treatments increased significantly the surface free energy to values of approximately 80 mN/m, i.e., the surfaces had a strong tendency to interact with liquids. In contrast, after applying the coating all studied surfaces showed a steep decrease in the surface free energy. The minimum measured value lied even below 1 mN/m and was obtained on the hierarchical textures.

To highlight the potential of glass surfaces with such extreme wettability contrast, a demonstrator was fabricated consisting of a spiral-like superhydrophilic channel surrounded by hydrophobic areas. The water released on one of the ends of the spiral is forced to wet and propagate through the channel. It is worth to point out that this demonstrator was fabricated at a total throughput of 1.5 cm^2/min, showcasing the scalability of the proposed process for industrial use. Moreover, in contrast to conventional fabrication techniques for open-surface microfluidics, such as photolithography, the proposed method eliminates the need for masks and post-processing steps involving chemical developers. Additionally, the presented approach uses a cost-effective ns-laser source instead of more costly fs-laser systems [11].

The results shown in this work can be further exploited for those applications in which controlled fluid manipulation is required in combination with high optical transparency such as in open-surface microfluidics or lab-on-a-chip devices. However, further studies must be carried out to evaluate this potential under realistic conditions including the use of relevant rheological or biological fluids and the performance characterization of channels with widths in the µm and sub-mm range.

Acknowledgments

This work was funded by the German Federal Ministry of Education and Research (BMBF), under the program WIR – GRAVOMER, project “03WIR2011”. The authors would like to thank C. Werner and R. Helbig (IPF, Dresden, Germany) for the assistance with SEM analysis; A. Kuntze and B. Mayr (Compact Laser Solutions GmbH, Berlin, Germany) for providing the laser source; and S. Kimme (Laservorm GmbH, Altmittweida, Germany) for the assistance with the construction of the setup.

References

[1] S. Xue, S. Yang, X. Li, Q. Li, and B. Hu: RSC Advances, 14, (2024) 34390.
[2] P. Sinha Mahapatra, R. Ganguly, A. Ghosh, S. Chatterjee, S. Lowrey, A. D. Sommers, and C. M. Megaridis: Chem. Rev., 122, (2022) 16752.
[3] Q. Wang, C. Liu, K. Yin, Y. Zhou, and H. Wang: Int. J. Appl. Glass Sci., 15, (2024) 57.
[4] H. Kozuka, Y. Miyao, T. Kato, and M. Miki: J. Sol-Gel Sci. Technol., (2024), DOI: 10.1007/s10971-024-06523-5.
[5] W. Wang and T. B. Jones: Lab Chip, 15, (2015) 2201.
[6] W.-H. Lin, C.-W. Chen, S.-H. Wang, and B.-R. Li: Sci. Rep., 11, (2021) 14915.
[7] M. Domke, G. Sonderegger, E. Kostal, V. Matylitsky, and S. Stroj: Appl. Phys. A, 125, (2019) 675.
[8] J. Zhang, B. Li, Z. Zhou, and J. Zhang: Small, 20, (2024) 2312112.
[9] L. Lu, L. Zhu, X. Liu, and J. Li: Chem. Eng. Res. Des., 188, (2022) 364.
[10] P. Premnath, A. Tavangar, B. Tan, and K. Venkatakrishnan: Exp. Cell Res., 337, (2015) 44.

[11] E. Kostal, S. Stroj, S. Kasemann, V. Matylitsky, and M. Domke: Langmuir, 34, (2018) 2933.
[12] Z. Bai, Q. He, S. Huang, X. Hu, and H. Chen: Anal. Chim. Acta, 767, (2013) 97.
[13] A. Peethan, J. Lawrence, and S. D. George: Int. J. Wett. Sci. Tech., 1, (2022) 189.
[14] E. Yu, S.-C. Kim, H. J. Lee, K. H. Oh, and M.-W. Moon: Sci. Rep., 5, (2015) 9362.
[15] B. Roy, A. Schmidt, A. Rosin, and T. Gerdes: Int. J. Appl. Glass Sci., 16, (2025) e16695.
[16] D. Zhang, N. Gao, W. Yan, W. Luo, L. Zhang, C. Zhao, W. Zhang, and D. Liu: Mater. Lett., 223, (2018) 1.
[17] S.-T. Wu, C.-Y. Huang, C.-C. Weng, C.-C. Chang, B.-R. Li, and C.-S. Hsu: ACS Omega, 4, (2019) 16292.
[18] P. R. Herman, R. S. Marjoribanks, A. Oettl, K. Chen, I. Konovalov, and S. Ness: Appl. Surf. Sci., 154–155, (2000) 577.
[19] R. Stoian, M. Boyle, A. Thoss, A. Rosenfeld, G. Korn, I. V. Hertel, and E. E. B. Campbell: Appl. Phys. Lett., 80, (2002) 353.
[20] J. Ihlemann and B. Wolff-Rottke: Appl. Surf. Sci., 106, (1996) 282.
[21] S. P. Sharma, R. Vilar, and R. Kumar: J. Non-Cryst. Sol., 636, (2024) 123021.
[22] M. Soldera, S. Alamri, P. A. Sürmann, T. Kunze, and A. F. Lasagni: Nanomaterials, 11, (2021) 129.
[23] A. F. M. Tahir, N. N. K. Azman, S. N. A. S. Ahmad, and I. Ismail: J. Adv. Res. Appl. Mech., 130, (2024) 80.
[24] A. F. M. Tahir, S. N. A. S. Ahmad, I. Ismail, N. E. M. Sariff, P. A.-S. Abdullah, and S. Abdullah: Jurnal Tribologi, 44, (2025) 16.
[25] K. A. N. Najwa, Z. Najihah, S. N. Aqida, I. Ismail, and M. S. Salwani: Int. J. Auto. Mech. Eng., 21, (2024) 10968.
[26] K. A. Nur Najwa, M. Hilmi, S. N. Aqida, and I. Ismail: J. Phys.: Conf. Ser., 2688, (2024) 012021.
[27] A. Ouchene, G. Mollon, M. Ollivier, X. Sedao, A. Pascale-Hamri, G. Dumazer, and E. Serris: Appl. Surf. Sci., 630, (2023) 157490.
[28] T.-H. Dinh, C.-V. Ngo, and D.-M. Chun: Appl. Phys. A, 126, (2020) 462.
[29] S. Razi, K. Madanipour, and M. Mollabashi: J. Laser Appl., 27, (2015) 042006.
[30] F. Ränke, S. Moghtaderifard, L. Zschach, R. Baumann, B. Voisiat, M. Soldera, L. Günther, S. Hilbert, C. I. Bernäcker, and T. Weißgärber: J. Laser Micro Nanoen., 19, (2024) 102.
[31] F. Hejda, P. Solar, and J. Kousal: Proc. WDS 2010, (2010) 25.

(Received: May 23, 2025, Accepted: August 3, 2025)